2013 American Control Conference (ACC)
Washington, DC, USA, June 17-19, 2013

Experimental verification of high speed AFM through local raster scanning

Peng Huang[1] and Sean B. Andersson[1,2]
[1]Department of Mechanical Engineering and [2]Division of Systems Engineering
Boston University, MA 02215

Abstract— **Local raster scanning is an algorithm for using the data acquired by an atomic force microscope in real time to steer the tip so that it stays on a sample of interest. The algorithm is suitable for all samples that are "string-like" in nature and has been shown through simulation and experiment to produce an order-of-magnitude improvement in imaging rate. This paper presents experiment results of applying the algorithm to gratings, demonstrating this improvement in speed. We compare the results to standard raster-scanning and discuss challenges introduced by our approach.**

I. INTRODUCTION

Atomic Force Microscopy (AFM) continues to play an essential role in the study of a wide variety of biological macromolecular systems. Examples include the direct observation of directional transport by protein motors [1], interactions between proteins [2], [3] and other cellular behaviors [4]. The importance and utility of this technology stems in part from its unique capabilities, including the ability to observe systems in their physiological environment, a resolution on the order of nanometers or better, and the ability to measure mechanical properties directly. One of the primary drawbacks of AFM when applying it to the study of dynamic processes, however, is its slow imaging rate with typical commercial instrument requiring seconds to minutes or longer to acquire a single high quality image. As a result, there is a great deal of ongoing work on increasing the speed of imaging. Approaches include improvements to the mechanical components [5], advanced controller designs for the piezo actuators [6], [7] and others such as using tuning forks for fast scanning [8] and novel detection-based approaches for imaging based on the transient response [9]. As a result, near video-rate speed has been achieved [10].

For some systems, however, even video-rate is not fast enough. For example, the dynein motor has been reported to move with a step size of 8 nm and at speeds of up to 1.7 μm per second [11]. At 30 frames per second, the motor would take approximately seven steps between the start and end of imaging a single frame. While the state-of-the-art in high speed AFM (HS-AFM) continues to advance, the drastic increase in speed needed for systems such as dynein argues for a different approach.

This work was supported in part by NSF through grant CMMI-0845742 and by grants from the Natiional Center for Research Resources (5R21RR025362-03) and the National Institute of General Medical Sciences (8 R21 GM103530-03) from the National Institutes of Health.

In prior work the authors (with others) introduced a Local Raster Scan (LRS) technique that reduces imaging time for string-like samples such as biopolymers [12]. The approach begins with the recognition that individual measurements in AFM are fast and that there is a lot of redundant information in conventional AFM images. Our algorithm, described in Sec. II, uses the measurements in real time to steer the tip of the AFM along the sample, focusing to the region of interest. The effectiveness of this algorithm was demonstrated in [12] using simulations and preliminary experiments in which the sample was replaced with a simulated model, omitting any dynamics of the cantilever, the tip sample interaction, and the controller of the z–piezo. These results indicated that an increase of at least an order of magnitude in the imaging rate can be expected for the particular class of samples described by string-like paths.

The algorithm is driven by the ability to detect when the tip of the AFM moves from substrate to sample or sample to substrate. In fact, by focusing on a problem of *detection* rather than imaging, the tip of the AFM can be moved along biopolymer samples at speeds far faster than can be used for imaging [14]. Since the quality of the various signals in the system depend on the tip speed, the choice of detector in turn must be made with this speed in mind. In this work we assume the AFM is in intermittent contact (tapping) mode and use either a simple threshold detector based on the amplitude signal or a transient signal method [9].

In order to analyze the cantilever motion for detection events, high sampling rates (well above the resonant frequency of the cantilever) are needed. Thus, while the computational requirements of our approach are not stringent, all computation must be done in a very short amount of time. We therefore chose to implement our algorithms in a field programmable gate array (FPGA) through the National Instruments compact Reconfigurable Input and Output (cRIO) system. The performance of the detectors at different tip speeds and experimental results on tracking the edges of both straight line and circular gratings using the LRS algorithm are illustrated.

II. LOCAL RASTER SCAN (LRS) ALGORITHM

The LRS algorithm is designed as a high-level feedback loop that closes the signal path between the measurements of the AFM and the commanded tip trajectory. It is primarily

designed for the high-speed imaging of dynamics along biopolymers and takes advantage of the structure in those systems to achieve significant gains in imaging rate. Details of the algorithm can be found in [12]; we give here only a brief description.

Under the LRS scheme, the tip is steered along a sinusoidal trajectory given by

$$x_{tip}(t) = x_{sample}(s(t)) + Aq_2(s(t))\sin(2\pi f s(t)) \qquad (1)$$

where x_{sample} is the predicted path of the sample based on the measurements, s is the arclength parameter of that path, further parameterized by time, $q_2(s)$ is the normal vector to the curve defined by the sample at the point s, A is a user-selected parameter defining the width of scanning, and f is a user-selectable parameter defining the spatial resolution of scanning. A detector determines if the tip is on the sample or substrate and flags the events when the tip moves from one to the other. Based on these crossing locations, the prediction of the curve x_{sample} is updated, closing the loop and keeping the tip moving along the sample. We have also developed a method to produce images from the local raster scan data based on interpolation; details can be found in [13].

As with standard raster-scanning, the frame rate of LRS is limited by several factors. Perhaps most important among them is the bandwidth of the mechanical components, including the nano-positioning system used. Since the technique is algorithmic, however, it can be utilized as an "add-on" module to existing, commercial AFMs to produce high speed imaging on non-high speed instruments (although limited to string-like samples). If the instrument used is itself already high speed then an additional order-of-magnitude increase in imaging rate can be achieved.

A. Choices of detectors

Good scanning with LRS begins with effective detection of whether the tip is on sample or off sample. In practice, the detector finds the edges of the sample in the scan; these edges are then used in the prediction of the sample's spatial evolution. In this paper, our focus is primarily on biological applications of HS-AFM and we therefore consider only the intermittent contact ("tapping") mode of AFM. The available signals for detection, in increasing order of bandwidth, are the output of the actuator in the z–direction (the height signal), the amplitude signal, and the motion of the cantilever itself. We note that the amplitude signal is analogous to the deflection signal in contact mode and the discussion below can be applied in that setting as well.

When imaging a sample, the output of the piezo actuator in the z–direction is often used to represent the sample profile. As such, it certainly contains information as to the edges of the sample in the scan. The signal, however, suffers from several drawbacks. Perhaps most notable is that the controller for the actuator produces overshoot and the system has vibrations that corrupt the height signal. Even at reasonable tip speeds, these artifacts can cause a high rate of false detection, quickly leading to loss of tracking under LRS. To avoid this scenario, the tip speed should be set slow enough so that the controller can return to steady state essentially instantaneously with respect to the measurement rate. Thus, the bandwidth of detection is limited by the (slow) bandwidth of the closed loop system. Further, the height signal is often corrupted by sample tilt (see, e.g. Fig. 2(a)) as well as by cross-coupling to the lateral motion of the actuation stage. While such effects can be overcome (and routinely are), the computational requirements are sufficiently high to make it difficult to compensate for them on-line during high speed scanning. Overall, these drawbacks are severe enough that the height signal is a poor choice for detection.

The second candidate signal for detection is the amplitude signal. The natural interpretation of this signal from a control point of view is as the error signal in the closed-loop system operating in tapping mode [15]. As the tip moves onto a sample from the substrate, the amplitude of the cantilever motion initially decreases before the controller regulates it back to nominal; as it moves off the sample and back to the substrate, the amplitude increases before the controller regulates it back to zero (see Fig. 2(b) for an example signal). The signal therefore contains information not only about the position of the edges but also about their direction. Further, detection can be achieved with a straightforward threshold detector. The detection speed, however, is closely coupled to the bandwidth of the closed-loop system. At very fast speeds, the controller has no time to respond and thus the amplitude signal becomes open loop, rendering meaningless the interpretation as an error signal.

At very fast tip speeds, then, neither the z–actuator signal nor the amplitude signal will work well, indicating that the image quality or the profile measured is not as credible as a low speed image. There are scenarios, however, where the profile information is well established but there is a dynamic process on that profile that is of interest. To address those applications, a discussion of derived signals of fast dynamics is presented below.

There is information in the dynamics of the cantilever motion that can be used to extract the position of the edges of the sample. To do this, we take advantage of a transient signal based detection method developed in [9]. The essential idea is to build a Kalman observer of the cantilever motion. Whenever the cantilever encounters a step-up (*e.g.* moving from substrate to sample), the system is assumed to have been subject to an abrupt change in state, leading to a mismatch between the initial condition of the observer and of the cantilever. The innovation signal of the observer, then, contains the information about the edges. To reliably detect these edges, the innovations are further processed using a maximum likelihood detector. This scheme can detect step-ups with a bandwidth one quarter of the resonant frequency of the cantilever [9], a rate that is decoupled from the speed of the piezo actuator or controller. The approach has difficulty detecting step-downs, however, primarily because the step down is poorly modeled as an abrupt change.

In this work we implemented the amplitude and transient signal approaches, selecting one or the other in a particular experiment based on the tip speed used (see Sec. IV-A).

III. Description of the Hardware Setup

The implementation of the LRS algorithm was done on a National Instruments cRIO9076. This system includes an embedded 400 MHz real-time processor and an LX45 FPGA from the Xilinx Spartan-6 family. The cRIO was outfitted with a 1Ms/s high-speed analog-digital converter (ADC) (NI 9215) for sampling the cantilever position, cantilever drive and the cantilever amplitude (deflection), a 100Ks/s ADC (NI 9223) for sampling the tip position and the z–controller output for the height information of the sample, a 100Ks/s digital-to-analog converter (DAC) to send out the tip trajectory calculated by the LRS, and a digital input and output (DIO) card for possible triggering applications. Software was written in LabView 12.0 (National Instruments).

A high level description of our design is as follows. There are three main blocks: the host computer, the real time process (RT), and the FPGA. Due to latency in transferring data between the real time processor and the FPGA, most of the algorithm was implemented in the FPGA despite the additional complexity of coding and debugging. The main role of the RT was to perform an initial raster scan to find a sample to track.

Note that in the trajectory in (1), the curve is specified with respect to arclength. The implementation, however, calculates in time, necessitating a conversion between time and arclength. The relationship involves an integral equation that depends on the parameters A and f and which, in general, must be solved numerically [12]. Performing this computation in real time in the FPGA is not feasible due to the numerical complexity of the solution. Thus a table of the the t–s relationship is calculated by the host system prior to beginning a run; this table is downloaded to the FPGA.

After receiving this table, the FPGA flags the host to go into an idle state and then sends in interrupt to the RT indicating that it should begin a standard raster scan. The RT does so until the tip encounters the sample. At that point, scanning is cancelled, the RT goes back to idle, and the FPGA and host enter their main loops.

The main loop of the FPGA performs detection, sample curve estimation (to generate the estimate x_d) and trajectory generation (x_{tip}). The detection loop executes at a rate of 500 Ks/s and runs either the amplitude threshold detector or the transient signal detector. Note that this high sampling rate necessitated that the FPGA executed under a generated clock of 80 MHz.

The estimation and trajectory generation loops are run at much slower rates, selected based on the desired tip sample rate (see the experiments in Sec. IV). Each time the detection loop flags the existence of an edge, these loops update the prediction of the sample path and the desired tip trajectory.

IV. Experiments

In this section we describe experimental results based on scanning of both a linear grating (TGZ01, MikroMash) and a circular grating (CS-20NG, Ted Pella). Each grating provided feature heights of 20 nm. The linear grating had a pitch width of approximately 3.3 μm while the circular grating had a pitch of 5 μm with circles of radius 3 μm. Standard raster-scan image of the gratings are shown in Fig. 4.

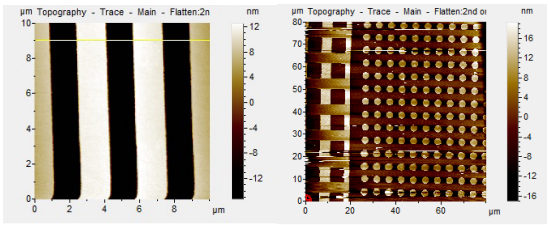

(a) Linear grating (b) Circular grating

Fig. 1. Standard raster-scan images of the (a) linear grating and (b) circular grating. Note that the circular grating is a portion of a larger grating sample and shows a region of a rectangular grating as well. Images acquired using an Agilent 5500 in AAC mode with a resolution of 256 × 256 pixels.

All experiments were performed using an Agilent 5500 AFM operated in AAC mode, a form of intermittent contact AFM. Agilent's z–controller was used, providing a bandwidth of around 10 kHz (as quoted by the manufacturer).

A. Effectiveness of the Detectors

In Fig. 2 we show both the height signal and the amplitude signal for a scan across the linear grating with a tip speed of 20 μm/s. The amplitude shows clear positive- and negative-going spikes as the tip moves over the edges in the sample. It is then straightforward to put a threshold detector to determine the position of those edges in the scan.

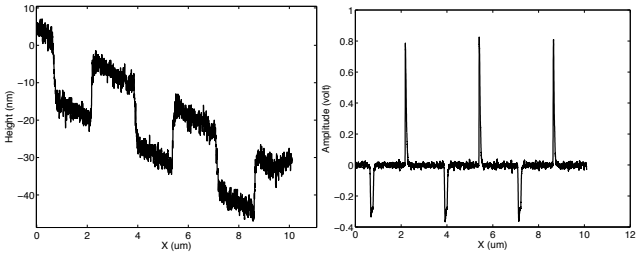

(a) z–controller output (height) (b) Amplitude signal

Fig. 2. (a) height and (b) amplitude signals for a scan across the linear grating in Fig. 4 with a tip speed of 20 μm/sec. Note that due to the nonlinear of the tip-sample interactions, the positive spikes are larger than the negative spikes.

The transient-based detector requires a model of the cantilever to formulate the Kalman observer. We used Agilent's built-in software to find the resonance frequency and quality factor of the cantilever and used those values to formulate a simple second-order model. In these experiments, the cantilever resonance frequency was 74.5 kHz and the quality factor was 210. The Bode plot is shown in Fig. 3(a). Since this detector was designed for fast tip speeds, we increased the speed to 4826 μm/sec, the upper limit of our instrument, and once again scanned the linear grating. The resulting innovation signal is shown in Fig. 3. This signal should be compared to the amplitude signal in 2(b). Note that the innovations show clear spikes, similar to the amplitude signal, but now only on the rising edges of the sample (note

the different pitch between the spikes). A threshold detector (although now with a disabling period after each detection to avoid false detections from the ring down of the observer) was again be used for detection. As noted in Sec. II-A, the innovation signal can be further filtered using a maximum likelihood detector if needed.

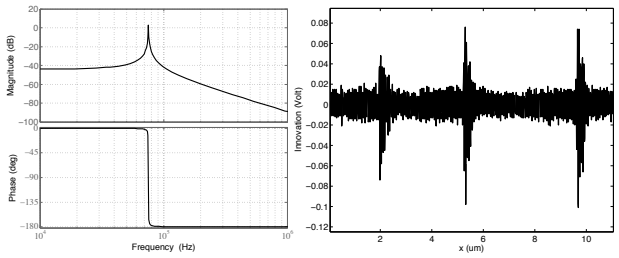

(a) Cantilever Bode plot (b) Innovation signal

Fig. 3. (a) Bode plot of the probe we used in the experiments and (b) innovation signal of a Kalman observer during a scan across the linear grating in Fig. 4 with a tip speed of 4826 μm/sec.

B. Straight Line Grating Test

In the remaining experiments, lateral scanning was performed using a two axis nanopositioning stage (two Nano-OP actuators mounted together, Mad City Labs) mounted underneath the AFM cantilever. This setup provided 30 μm of travel in the lateral directions and allowed us to easily specify our own trajectories while taking advantage of the z–controller in the AFM. The stages were operated using the manufacturer provided closed loop controller, yielding a bandwidth of less than 100 Hz in both the x and y directions.

In this section we report on an experiment demonstrating the LRS algorithm scanning an edge in the linear grating. A raster-scan of the grading and a box of the region of interest are shown Fig. 4. The amplitude parameter of the LRS was set to A =1.35 μm and the spatial frequency to f =1/80 nm^{-1}. Note that the scan crosses the sample twice per period so the effective resolution in the scan is 40 nm between crossings along the edge.

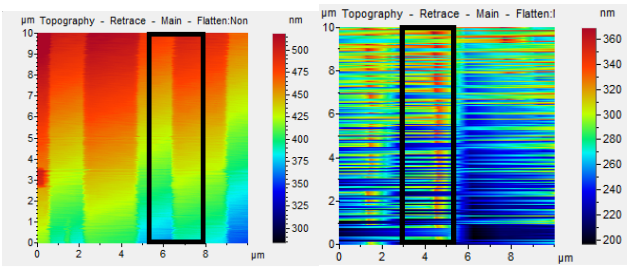

(a) Slow scan (b) Fast scan

Fig. 4. (a) Raster image of the grating sample at a tip speed of 11.2 μm/sec.The scan range was 10 μm and the number of pixels per line was set to 256 to obtain the same resolution as in the local raster scan.(b) Raster imaging of the grating sample at a tip speed of approximately 120 μm/sec and at the same resolution. There is little information in the image.

Two scans are reported. In the first the tip speed was set to 11.2 μm/sec. In this run the threshold detector on the amplitude signal was used and all signals were sampled at 1 kHz. The results are shown in Fig. 5. The figure shows the x–y trajectory of the tip, the height image of the edge generated from the data collected along the trajectory, and the height signal, amplitude signal, and detection signal. The scan took 34 seconds to complete. The generated image clearly shows the edge as well as the overall sample tilt. We note that no post-processing was run on the data; typically one would flatten the image to remove the sample tilt.

To place these results in context, a standard raster scan was performed using the Agilent 5500 AAC mode. An image size of 10 μm square was selected with the line rate of 0.5 Hz was selected to match (approximately) the tip speed of 11.2 μm/sec and an image size of 256 pixels square was selected to match the 40 nm resolution in the LRS image. Note that in standard raster imaging, a single line consists of a trace and a retrace scan; thus a line rate of 0.5 Hz translates to 10 μm/sec tip speed. The resulting image is shown in Fig. 4(a). To compare the results, the region scanned by the LRS algorithm is boxed in black; this region took 422 seconds to image using standard raster scanning. The images created by the LRS algorithm and the raster scan compare quite well despite the fact that LRS was an order of magnitude faster.

In the second scan the tip speed was set to 112 μm/sec; the amplitude and resolution parameters were left unchanged. The rate of sampling (and the closed-loop control rate) was increased to 10 kHz. A standard raster scan was performed at a line rate of 6 Hz to match the tip speed; the result is shown in Fig. 4(b). This scan speed is clearly too fast for the controller and the resulting image is nearly meaningless. Also shown on the image is the region scanned using the LRS algorithm as discussed below. The equivalent time for the standard raster scan of this area was 41 seconds.

The LRS results are shown in Fig. 6. The threshold detector on the amplitude signal was used for detection. The trajectory, shown in Fig. 6(a) follows the edge of the grating despite the poor height data, completing the scan in 3 seconds. This poor data is reflected in the image generated from the measurements, shown in Fig. 6; the result is similar to the regular raster scan image. The conclusion to be drawn is that tracking of features can be done successfully at rates beyond what is needed for good imaging, opening up the possibility of tracking dynamic changes along such features.

C. Circle Grating Test

In this section we show the results of applying the LRS to the circular grating. The first run shown is for a sampling rate of 1 kHz, a tip speed of 37 μm/sec, an amplitude of A= 1.12 μm and a spatial frequency of f = 1/40 nm^{-1} (corresponding to a spatial resolution of 20 nm). Fig. 7 shows the tip trajectory, the generated image, and the height, amplitude, and detection signals. As shown in Fig. 7(d), the height data was poor and therefore an image was generated from the amplitude signal. As before the threshold detector on the amplitude signal was used. The run began on the top of the circle and proceeded clockwise around. Due most likely to debris, tracking was lost after proceeding approximately

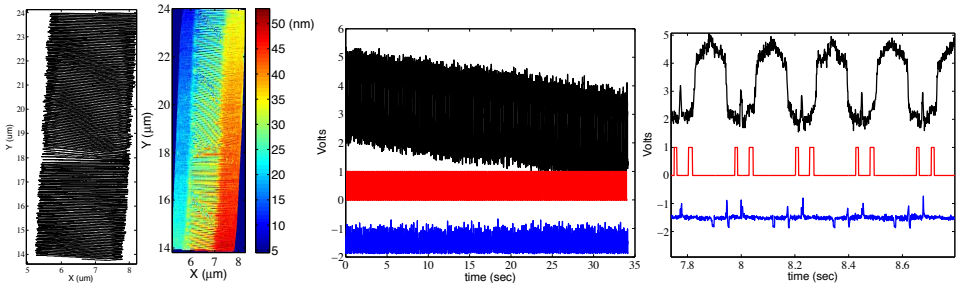

(a) X-Y (b) Imaging (c) *Z*-direction signals (d) *Z*-direction signals zoom in

Fig. 5. LRS scan of a linear grating using a tip speed of 11.2 μm/sec. (a) tip trajectory; (b) image generated from the data acquired along the tip trajectory in (a); (c) measured signals: height (in black), amplitude (in blue), and detector (with 0 indicating no detection, 1 indicating detection) (red); (d) zoomed-in version of the signals in (c) to better show their features.

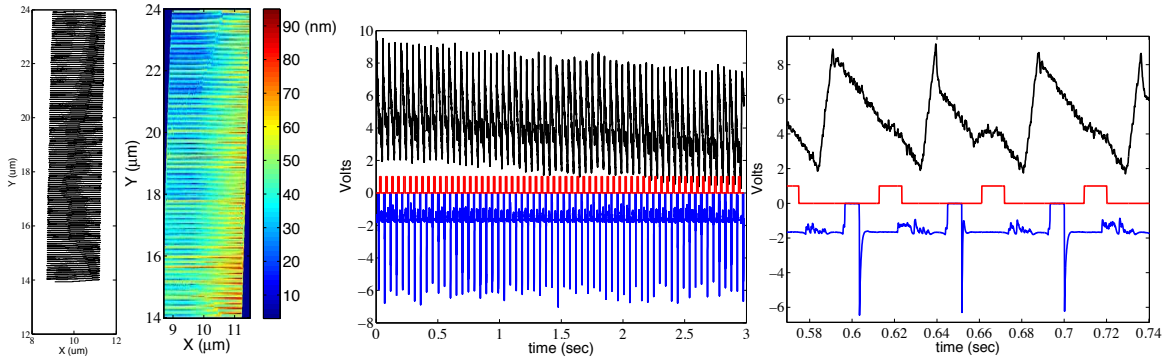

(a) X-Y (b) Imaging (c) *Z*-direction signals (d) *Z*-direction signals zoom in

Fig. 6. Illustration of the results of 10kHz sampling rate run. (a) tip trajectory; (b) image generated from the data acquired along the tip trajectory in (a);measured signals: height (in black), amplitude (in blue), and detector (with 0 indicating no detection, 1 indicating detection) (red); (d) zoomed-in version of the signals in (c) to better show their features.

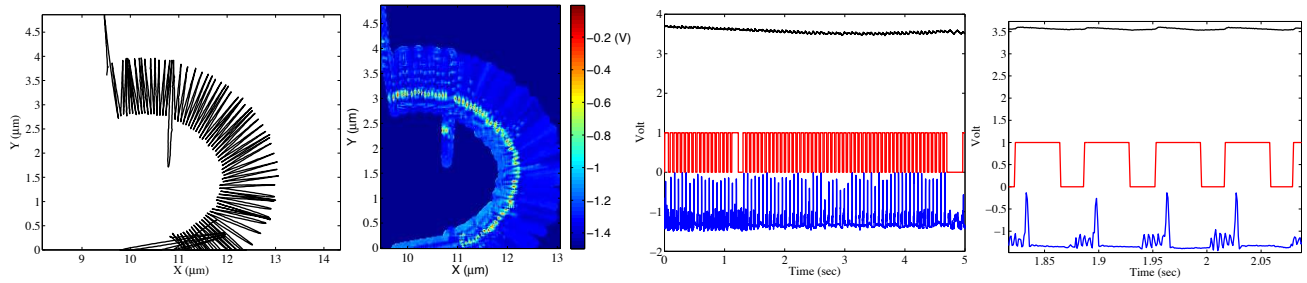

(a) Tip trajectory (b) Imaging of grating (c) *Z*-direction signals (d) *Z*-direction signals zoom in

Fig. 7. LRS scan of a circular grating using a tip speed of 37 μm/sec. (a) tip trajectory; (b) image generated from the data acquired along the tip trajectory in (a); (c) measured signals: height (black), amplitude (blue), and detector (with 0 indicating no detection, 1 indicating detection (red); (d) zoomed-in version of the signals in (c) to better show their features.

halfway around the circle. (See also the discussion in Sec. IV-D). This scan took approximately five seconds; an equivalent raster-scan image would take 85 seconds.

In the second run, the sampling rate was increased to 10 kHz and the tip speed to 74 μm/sec; other parameters were unchanged. The results are shown in Fig. 8. Scanning was done counter clockwise. As before, tracking was lost approximately halfway around the circle, likely due to dust or debris. This scan took approximately 2.5 seconds while an equivalent standard raster-scan would take 43 seconds. The generated image is based on the amplitude signal.

D. Challenges for a successful tracking

Unlike the standard raster-scan pattern, the LRS algorithm is a closed-loop law that relies on the current measurements to drive the tip trajectory. This leads to the order-of-magnitude improvement in scanning time shown experimentally above, but also introduces new challenges due to noise and unmodeled events in the scanning. This is clear from the two circular trajectory scans in Figs. 7,8 in which tracking was lost before the feature was fully scanned.

In Fig. 9 we show a standard raster scan (height and amplitude images) of one of the circular features. The

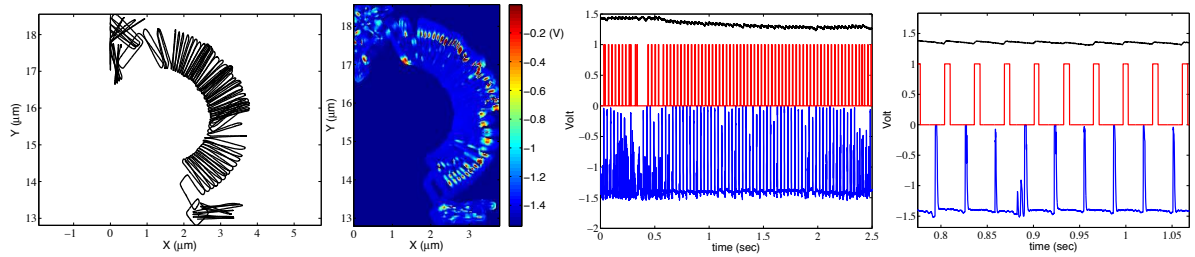

(a) Tip trajectory (b) Imaging of grating (c) Z-direction signals (d) Z-direction signals zoom in

Fig. 8. LRS scan of a circular grating using a tip speed of 74 μm/sec. (a) tip trajectory; (b) image generated from the data acquired along the tip trajectory in (a); (c) measured signals: height (black), amplitude (blue), and detector (with 0 indicating no detection, 1 indicating detection (red); (d) zoomed-in version of the signals in (c) to better show their features.

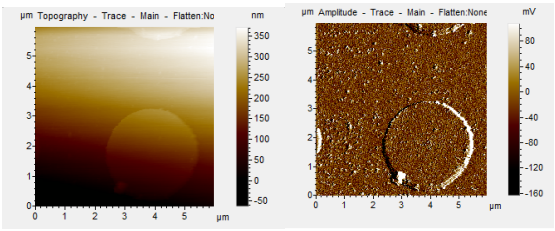

(a) Height image (b) Amplitude image

Fig. 9. Raster-scan image of a circular grating at an equivalent tip speed of approximately 37 μm/sec.(a) Height image; (b) Amplitude image.

amplitude image in particular indicates a number of scratches and dust that are rife over the surface. The detector cannot distinguish *what* causes a spike in the amplitude signal (or innovations signal) and therefore any of these could trigger a false detection. While there is some filtering in the algorithm, such false triggers, if far away from the actual feature, can cause immediate loss of tracking. The solutions to these issues rely on how to acquire and make use of necessary prior knowledge of the sample under scanned and are the topic of active investigation.

A second problem is the tilt of the sample, shown clearly in Fig. 9. In standard imaging such tilt is removed using post-processing. In the LRS, the detectors nominally are independent of the sample tilt; however, the performance of the z–controller is impaired if the rate of tilt is fast with respect to the size of the scan. This directly leads to poor detector performance.

V. CONCLUSIONS

This paper presented the first experimental results from the LRS algorithm. The results show the algorithm can yield an order-of-magnitude reduction in imaging time simply by focusing the measurements on the sample. The experiments also demonstrate, however, that it is important that the sample be as free of debris as possible to prevent false detections and loss of tracking. While this seems restrictive, even in standard raster-scan imaging such steps are routinely taken to ensure a high-quality image. For example, images of DNA are often acquired using freshly cleaved mica as a substrate so that the DNA lies on an atomically flat surface. We are also considering methods for improving the robustness of the algorithm with respect to such disturbances.

REFERENCES

[1] N. Kodera, D. Yamamoto, R. Ishikawa, and T. Ando, "Video imaging of walking myosin V by high-speed atomic force microscopy," *Nature*, vol. 468, pp. 72–76, Oct 2010.

[2] O. H. Willemsen, M. M. E. Snel, A. Cambi, J. Greve, B. G. D. Grooth, and C. G. Figdor, "Biomolecular interactions measured by atomic force microscopy," *Review of Scientific Instruments*, vol. 79, no. 6, pp. 3267–3281, Dec 2000.

[3] M. B. Viani, L. I. Pietrasanta, J. B. Thompson, A. Chand, I. C. Gebeshuber, J. H. Kindt, M. Richter, H. G. Hansma, and P. K. Hansma, "Probing protein–protein interactions in real time," *Nature Structural Biology*, vol. 7, no. 8, pp. 644–647, Aug 2000.

[4] T. Ando, T. Uchihashi, N. Kodera, D. Yamamoto, A. Miyagi, M. Taniguchi, and H. Yamashita, "High-speed AFM and nano-visualization of biomolecular processes," *Eur J Physiol*, vol. 456, pp. 211–225, Dec 2008.

[5] G. E. Fantner, G. Schitter, J. H. Kindt, T. Ivanov, K. Ivanova, R. Patel, N. Holten-Andersen, J. Adams, P. J. Thurner, I. W. Rangelow, and P. K. Hansma, "Components for high speed atomic force microscopy," *Ultramicroscopy*, vol. 1, no. 15, pp. 1–7, Jan 2004.

[6] G. Schitter, F. Allgower, and A. Stemmer, "A new control strategy for high-speed atomic force microscopy," *Nanotechnology*, vol. 15, pp. 108–114, Nov 2004.

[7] S. Salapaka, A. Sebastian, J. P. Cleveland, and M. V. Salapaka, "High bandwidth nano-positioner: A robust control approach," *Review of Scientific Instruments*, vol. 73, no. 9, pp. 3232–3241, Sep 2002.

[8] L. M. Picco1, L. Bozec, A. Ulcinas, D. J. Engledew, M. Antognozzi, M. A. Horton, and M. J. Miles, "Breaking the speed limit with atomic force microscopy," *Nanotechnology*, vol. 18, pp. 1–4, Dec 2006.

[9] S. Salapaka, T. De, and A. Sebastian, "Sample-profile estimate for fast atomic force microscopy," *Applied Physics Letters*, vol. 87, p. 053112 (3 pages), July 2005.

[10] G. Schitter and M. J. Rost, "Scanning probe microscopy at video-rate," *Materials Today, Microscopy special issue*, pp. 40–48, 2009.

[11] C. Kural, H. Kim, S. Syed, G. Goshima, V. I. Gelfand, and P. R. Selvin, "Kinesin and dynein move peroxisome in vivo: a tug-of-war or coordinated movement?" *Science*, vol. 308, no. 5727, pp. 1469–1472, June 2005.

[12] P. Chang, P. Huang, J. Maeng, and S. Andersson, "Local raster scanning for high speed imaging of biopolymers in atomic force microscopy," *Review of Scientific Instruments*, vol. 82, no. 6, p. 063703 (7 pages), June 2011.

[13] P. Huang and S. B. Andersson, "Generating images from non-raster data," in *Proceedings of the American Control Conference*, San francisco, CA, June 2011, pp. 2246–2251.

[14] ——, "Fast detection based on semi-transient signals in afm," in *Proceedings of the American Control Conference*, Montreal, CANADA, June 2012, pp. 3216–3221.

[15] D. Y. Abramovitch, S. B. Andersson, L. Y. Pao, and G. Schitter, "A tutorial on the mechanisms, dynamics, and control of atomic force microscopes," in *Proceedings of the 2007 American Control Conference*. New York City, USA: American Control Conference, July 2007, pp. 3488–3502.